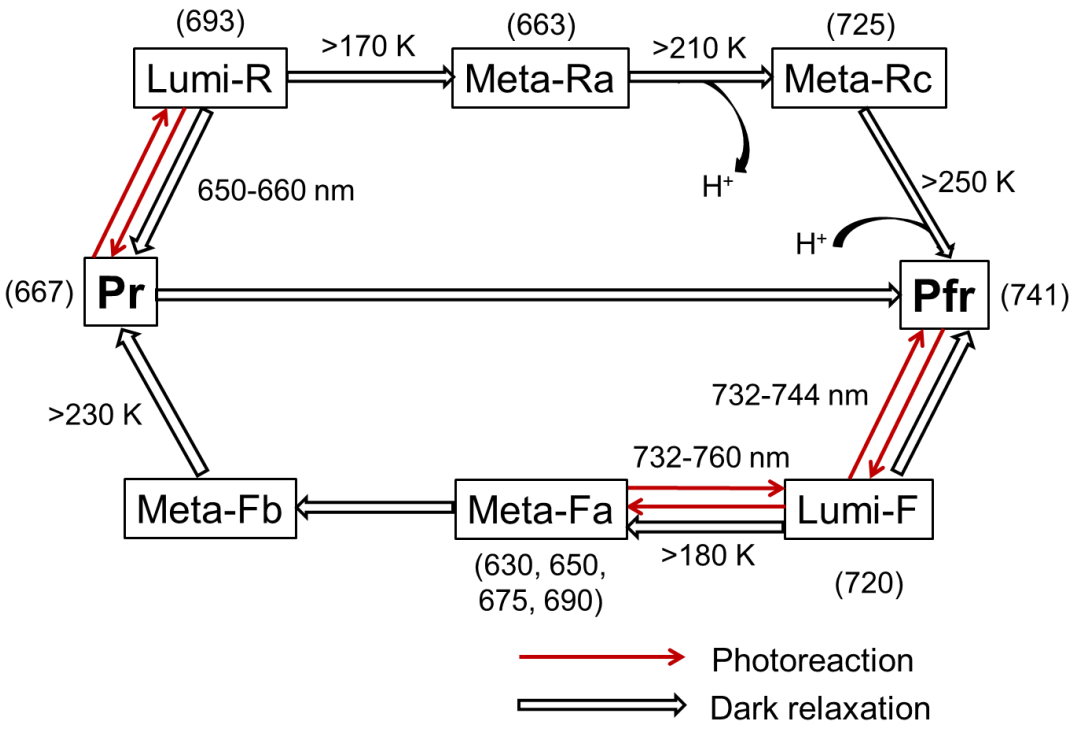

Supplementary Figure S1. Schematic representation of the phytochrome photocycle. The scheme is adopted from the references[12, 13, 15, 47, 48]. Values in the brackets denote wavelength of difference spectrum peaks. Indicated temperatures correspond to the minimum values for the individual relaxation steps.

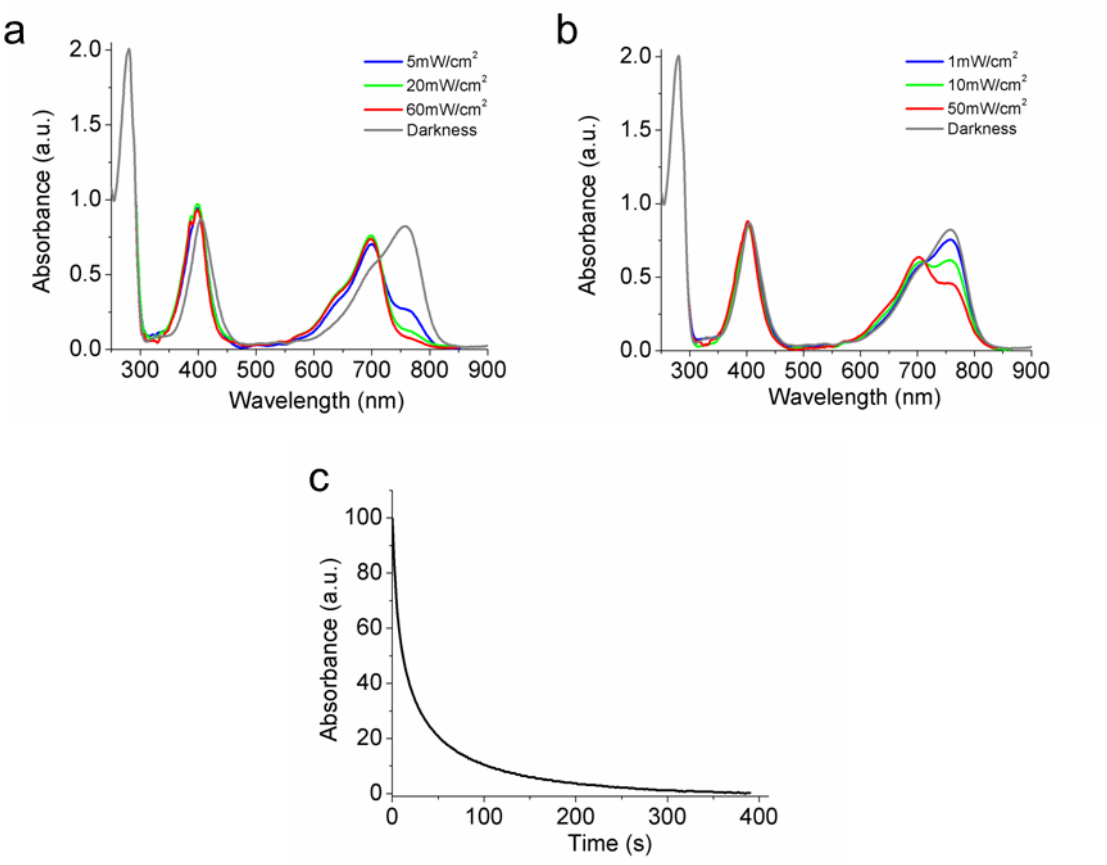

Supplementary Figure S2. Photoconversion of the purified AtPCD protein. The sample of completely relaxed AtPCD (gray line) was illuminated for 10 s in a 150 µl cuvette by either (a) 750 nm or (b) 660 nm LED light of different intensities. Absorbance spectra were measured under continues illumination. (c) Dark reversion of AtPCD after illumination with 750 nm LED light assayed by measurements of absorbance at 699 nm.

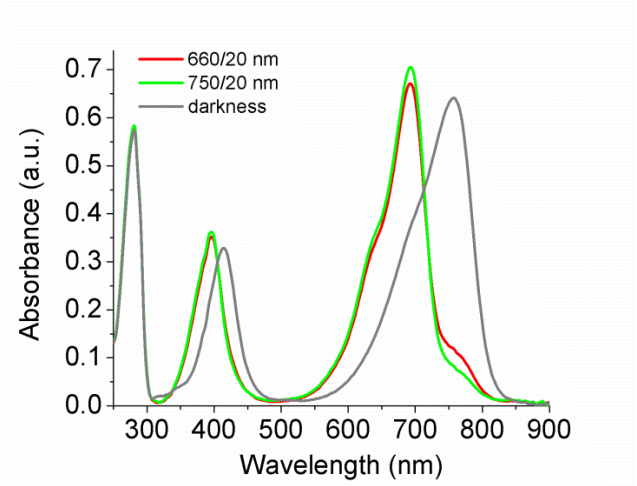

Supplementary Figure S3. Photoconversion of the purified At/660-I#1 mutant. The sample of completely relaxed At/660-I#1 (gray line) was illuminated for 10 s in a 150 µl cuvette by either 660 nm of 50 mW/cm^2 (red line) or 750 nm of 60 mW/cm^2 (green line) LED light. Absorbance spectra were measured immediately after the illumination.

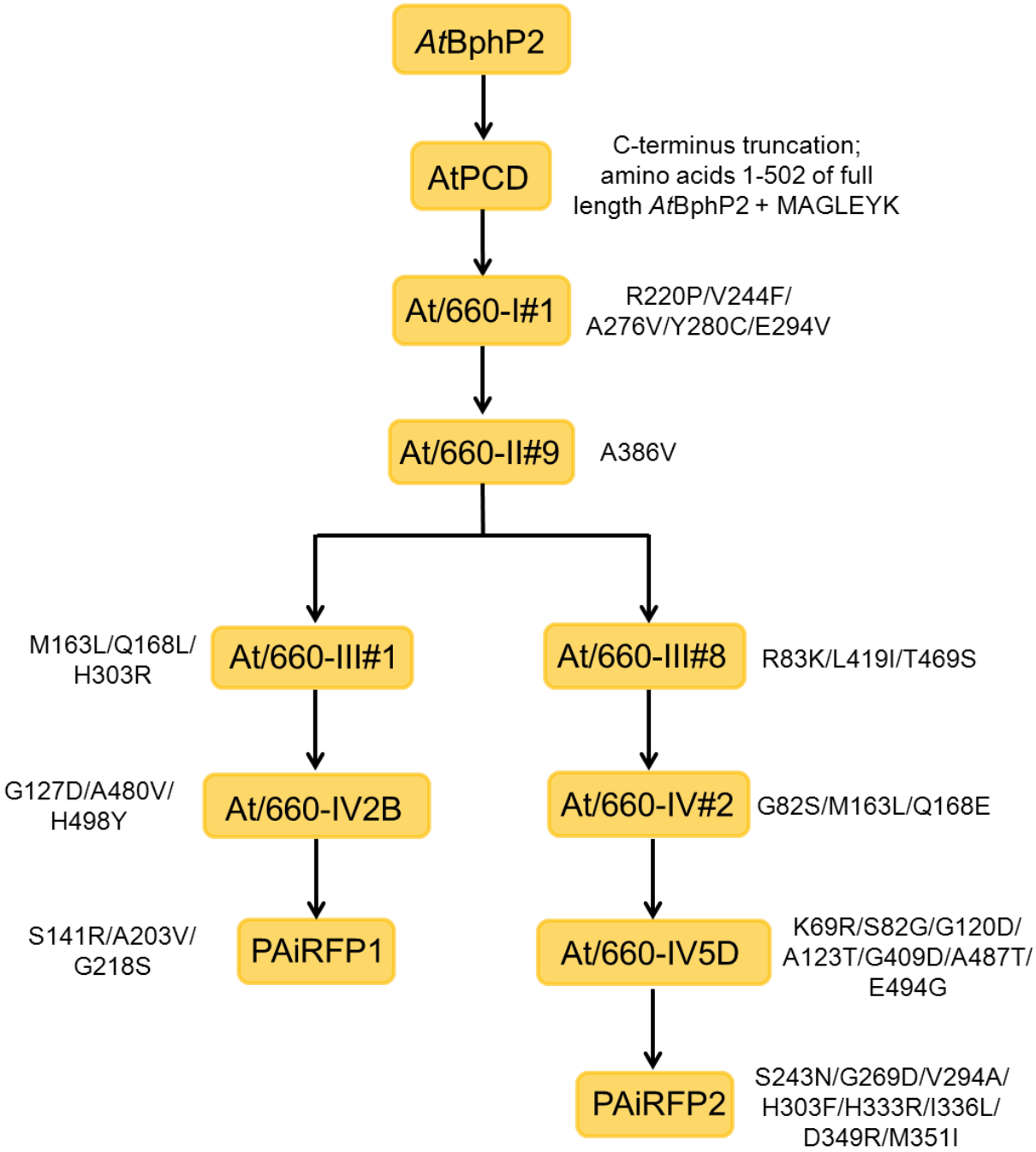

Supplementary Figure S4. Molecular evolution of PAiRFPs showing protein modification and amino acid mutations introduced during each round.

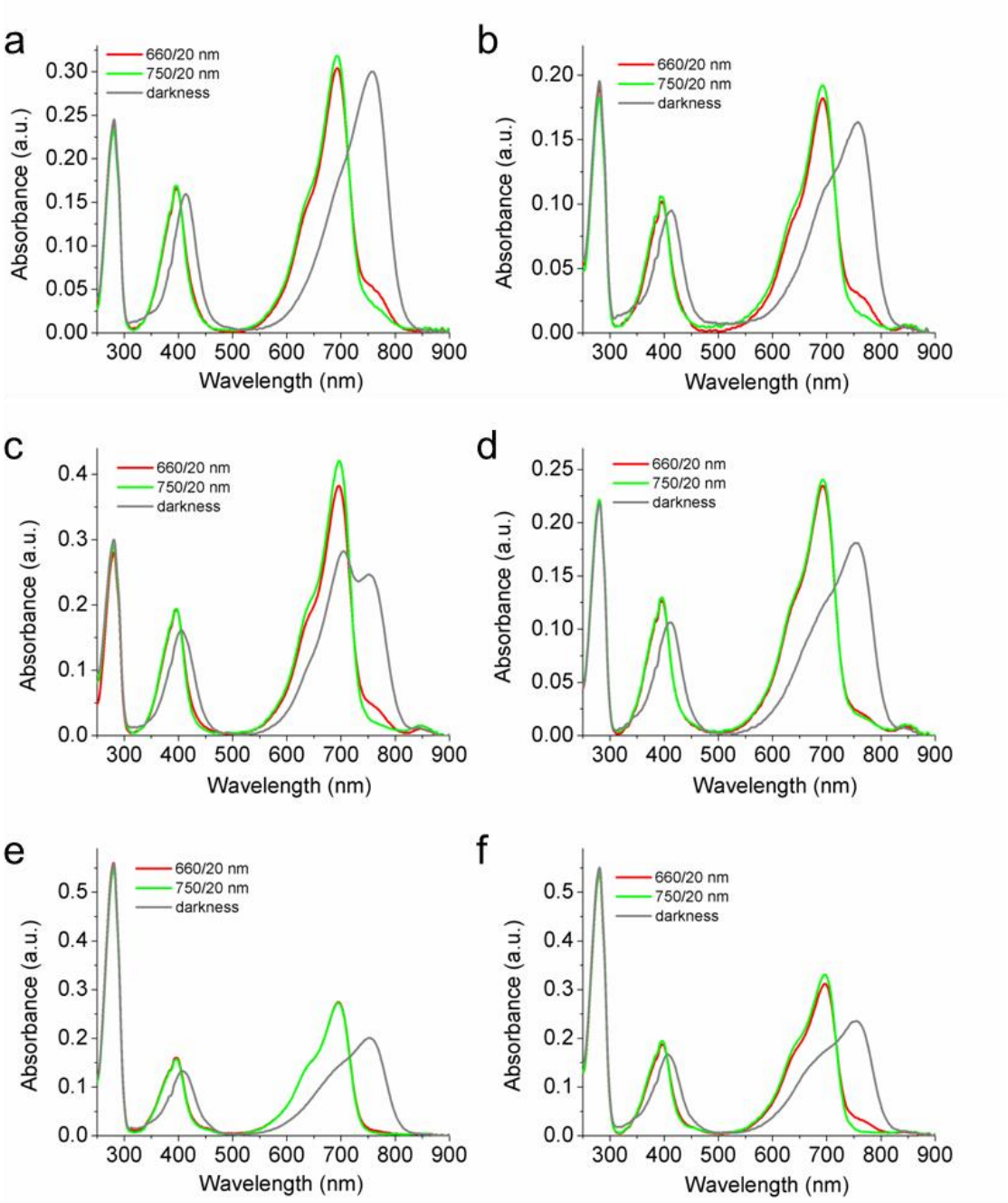

Supplementary Figure S5. Photoconversion of the purified PAiRFP precursors. (a) At/660-II#9, (b) At/660-III#8, (c) At/660-II#9QCH#1, (d) At/660-IIIQCH#2, (e) At/660-IV2B and (f) At/660-IV5D mutants were measured after 10 s illumination in a 150 µl cuvette with 50 mW/cm^2 of 660 nm or 60 mW/cm^2 of 750 nm LED light. Absorbance was measured immediately after the illumination. Absorbance of the relaxed proteins is shown by gray lines.

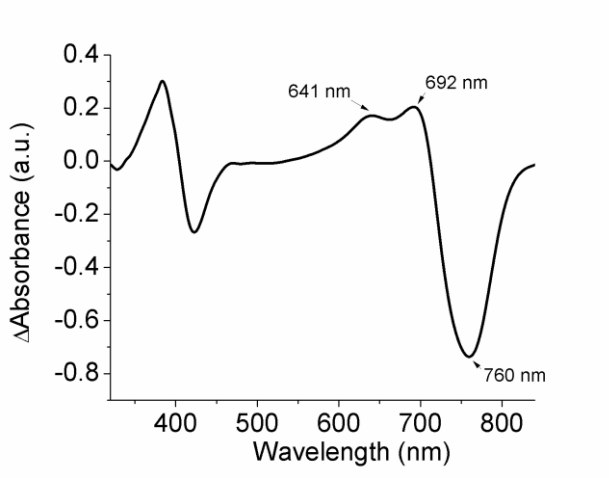

Supplementary Figure S6. Difference spectra for phototransformation of AtPCD. Difference spectra "relaxed" minus "photoactivated" for AtPCD. Photoactivation was performed by 60 mW/cm^2 of 750 nm LED light.

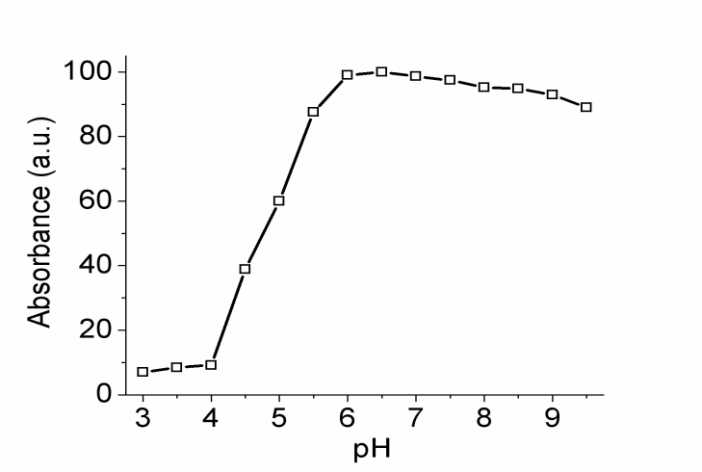

Supplementary Figure S7. The pH stability of the Pfr form of AtPCD. Absorbance changes were recorded at 758 nm.

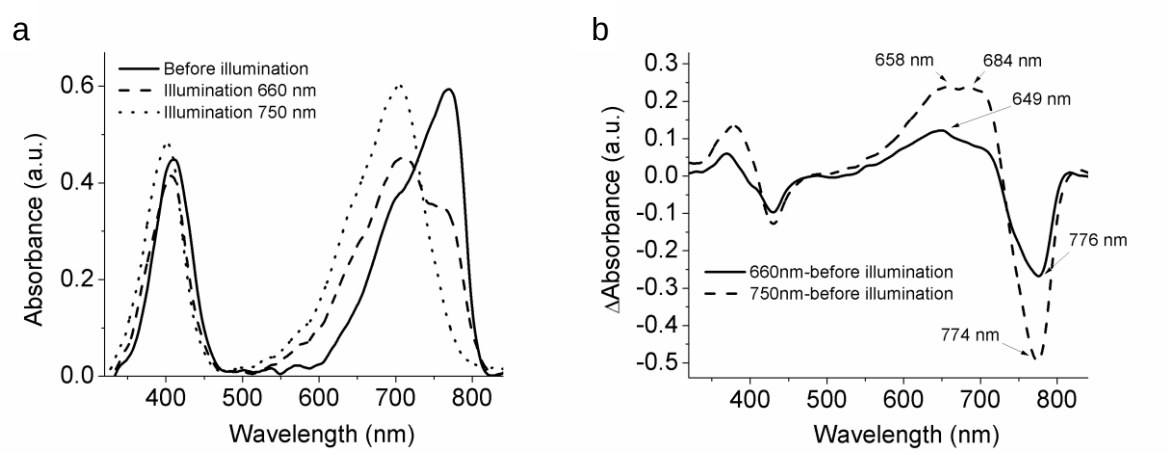

Supplementary Figure S8. Low temperature UV-visible spectroscopy of intermediate products of AtPCD photoconvertion.(a) Absorbance spectra of relaxed AtPCD measured at 77 K before illumination (solid line), after 10 s of 660 nm LED illumination (dashed line), and after 10 s of 750 nm LED illumination (dotted line). (b) Difference spectra for phototransformation of relaxed AtPCD at 77 K: “660 nm illumination” minus “before illumination” (solid line), and “750 nm illumination” minus “before illumination” (dashed line).

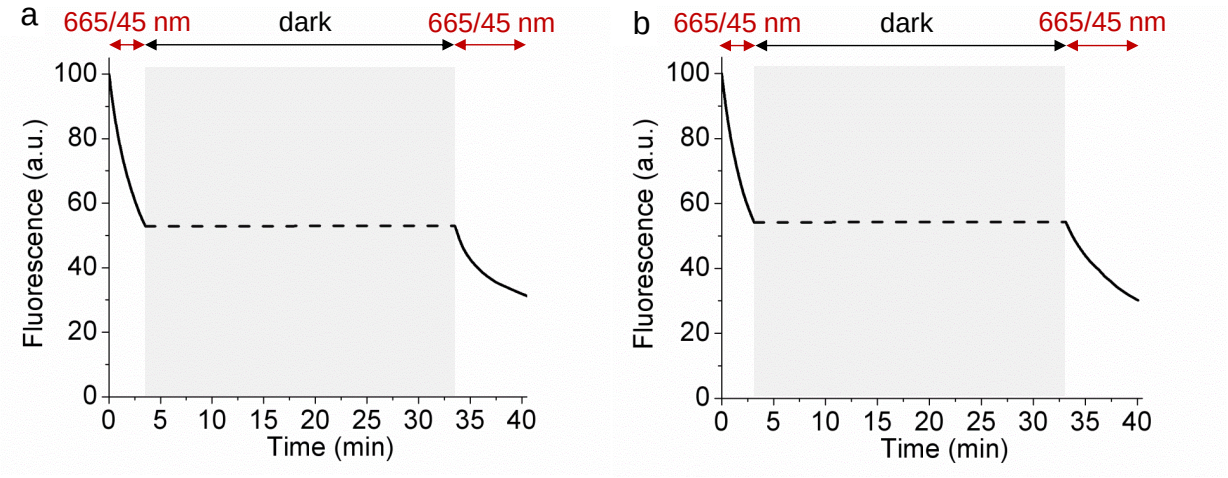

Supplementary Figure S9. Irreversible photobleaching of PAiRFPs in mammalian cells. Live Met-1 cells stably expressing either PAiRFP1 (a) or PAiRFP2 (b) were irradiated under an Olympus IX81 inverted epifluorescence microscope equipped with a 200 W metal-halide arc lamp (Prior), a 60x 1.35 NA oil immersion objective lens (UPlanSApo, Olympus), and 665/45 nm filter (Chroma). Single cells were photobleached using the highest achievable at this wavelength range light intensity of 8.9 mW/cm^2, which was measured at a back focal plane of the objective lens. Cells expressing PAiRFPs initially photobleached for 3.5 min (0-3.5 min) were kept in a dark for 30 min (3.5-33.5 min) and then photobleached again for additional 6.5 min (33.5-40 min).

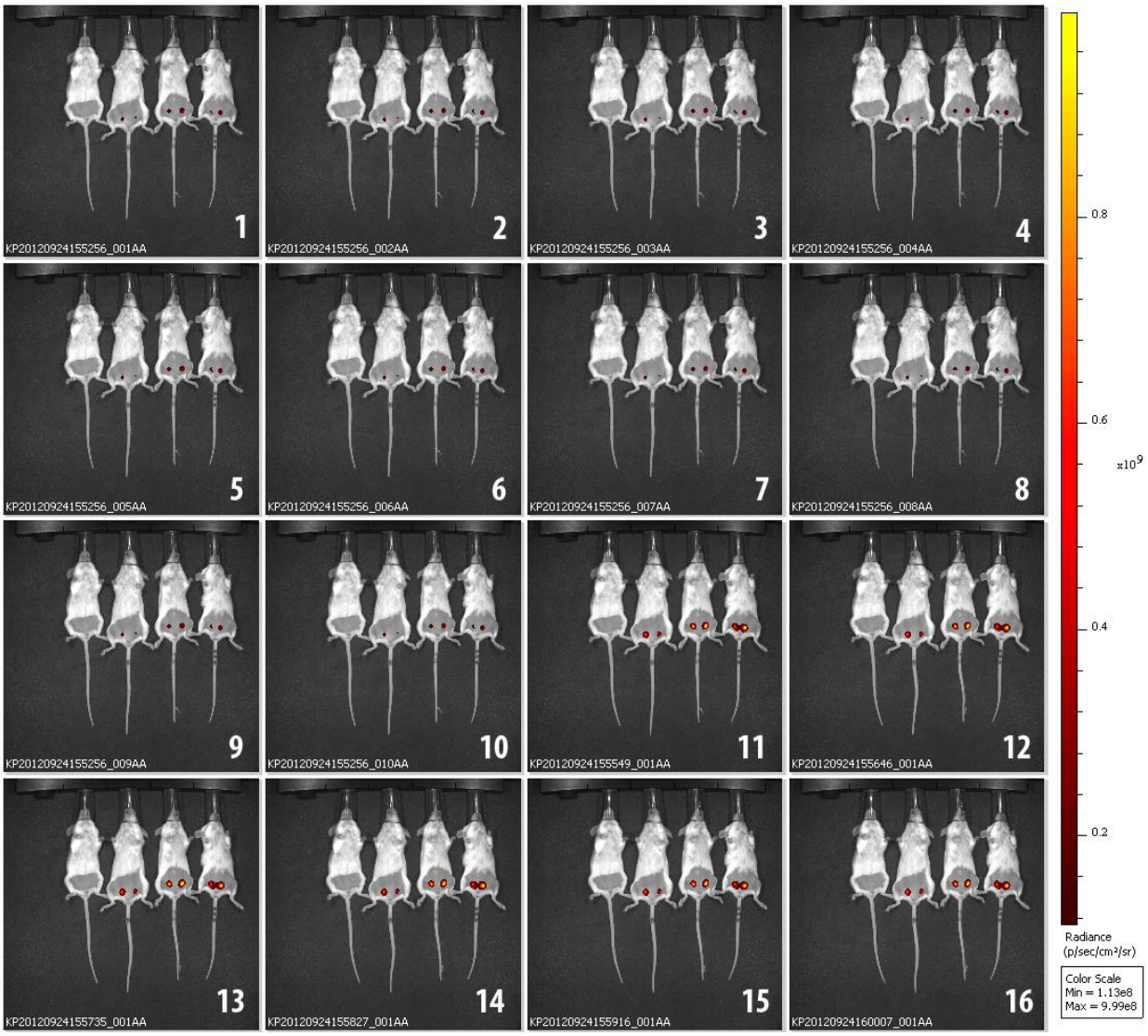

Supplementary Figure S10. Photoactivation of PAiRFP1 expressing tumor under 660 nm LED array.Sequence of the overlays of the representative light and fluorescent images of control mouse (left one on each image) and mice bearing the 11 day old MTLn3 tumor expressing PAiRFP1. The mice were imaged with 675/30 nm 6.4 μW/cm^2 excitation light (2 s exposure time per frame) before (frames 1-10) and after repetitive 5 s irradiation with 660 nm 26 mW/cm^2 LED photoactivation light per each frame (frames 11-16).

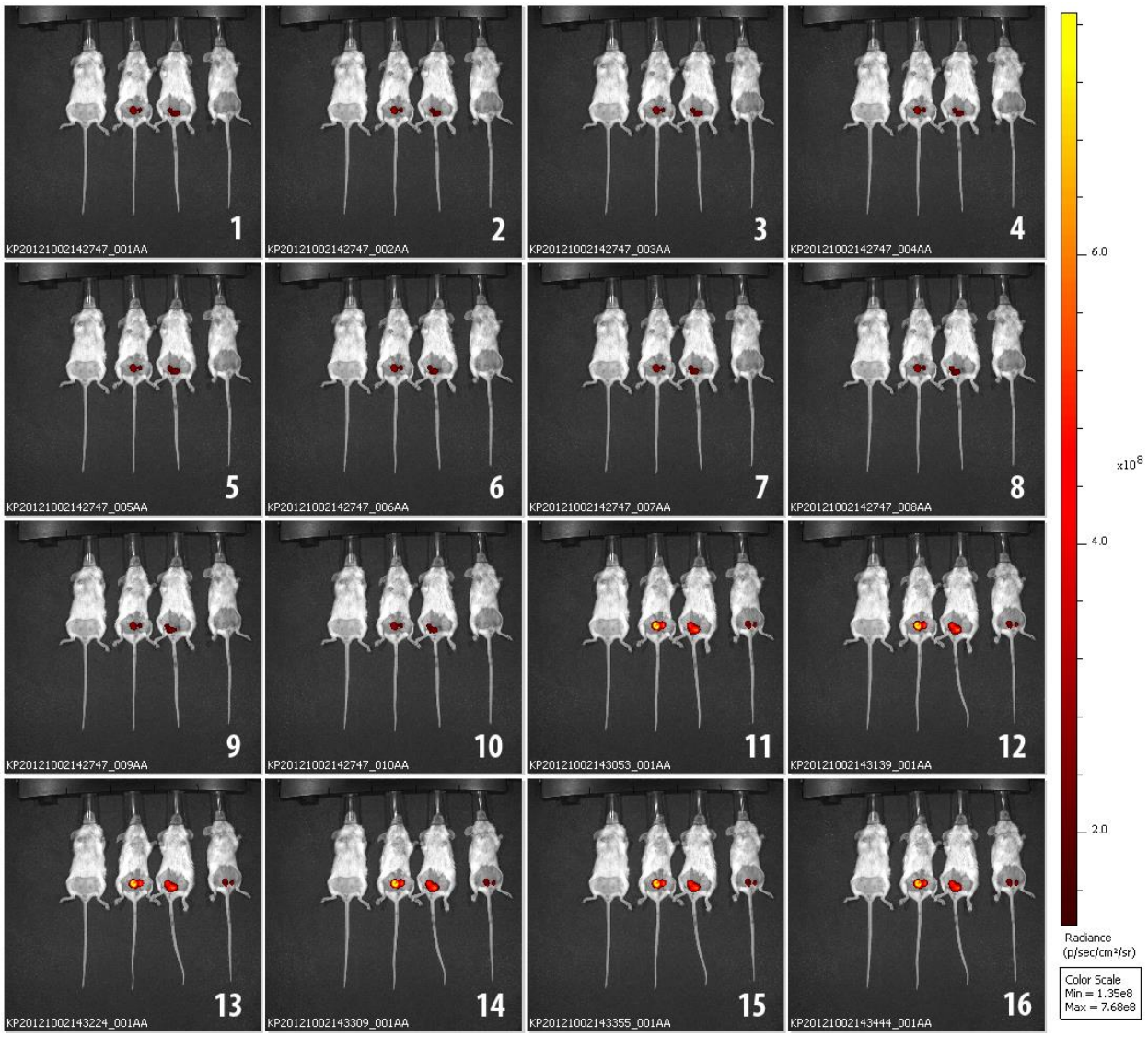

Supplementary Figure S11. Photoactivation of PAiRFP2 expressing tumor under 660 nm LED array. Sequence of the overlays of the representative light and fluorescent images of control mouse (left one on each image) and mice bearing the 18 day old MTLn3 tumor expressing PAiRFP2. The mice were imaged with 675/30 nm 6.4 μW/cm^2 excitation light (2 s exposure time per frame) before (frames 1-10) and after repetitive 5 s irradiation with 660 nm 26 mW/cm^2 LED photoactivation light per each frame (frames 11-16).

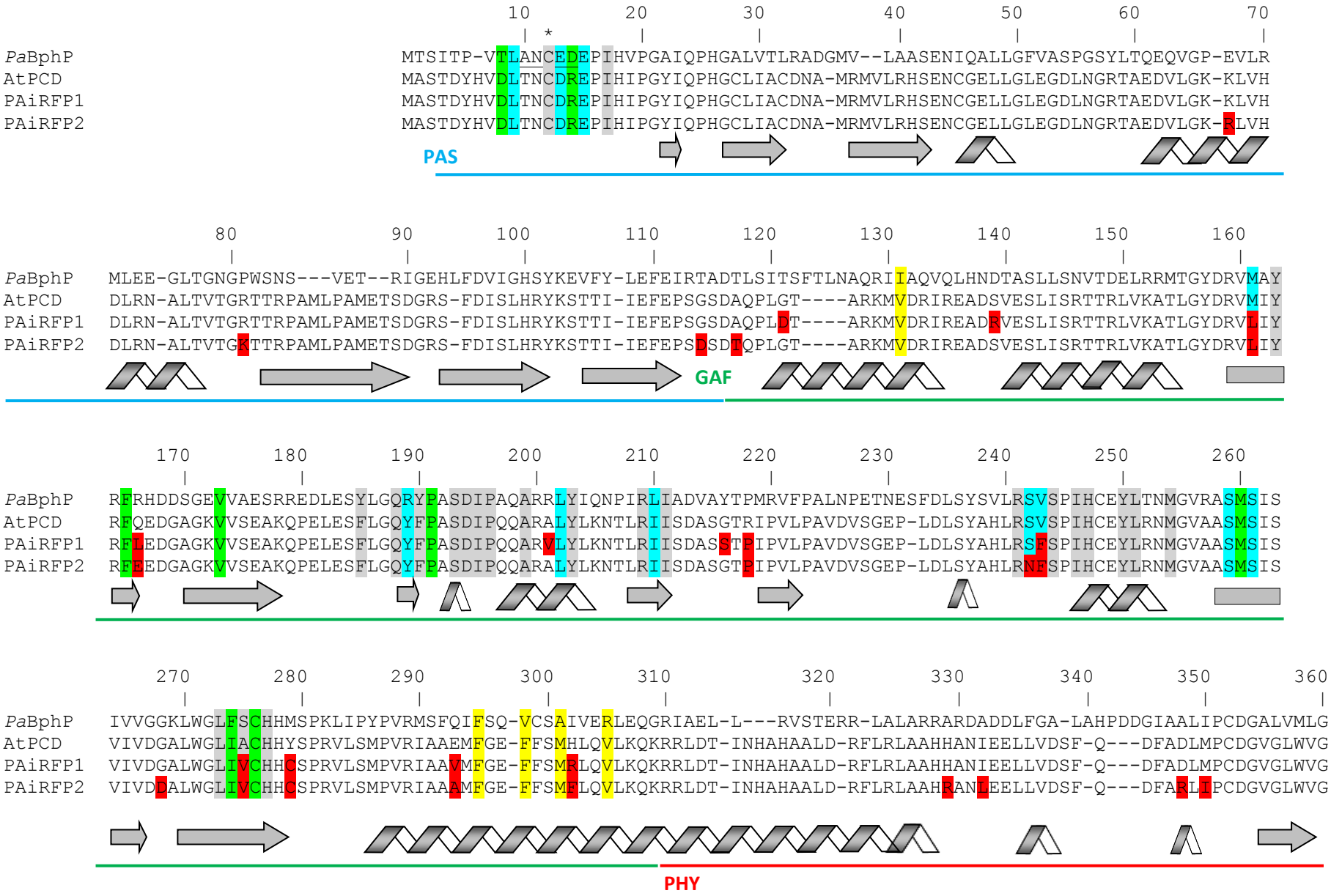
PAS
GAF
PHY

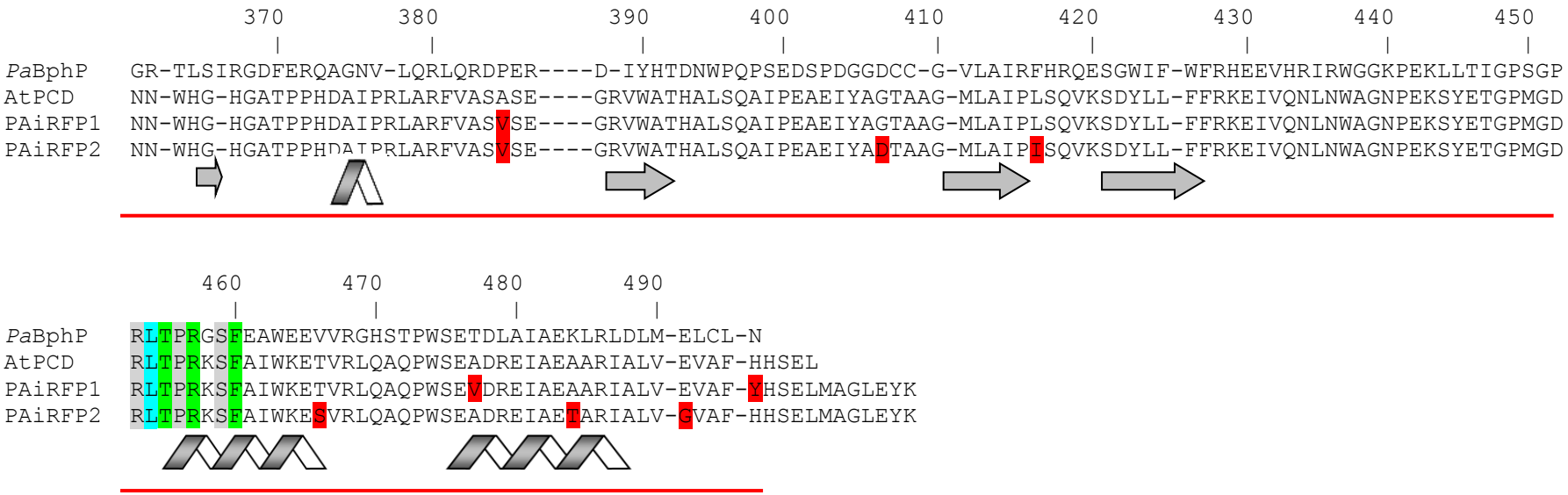

Supplementary Figure S12. The amino acid sequence alignment for the AtPCD, PAiRFPs, and *Pa*BphP PCD. The numbering of amino acid residues follows that for *Pa*BphP protein. Cys residue, which is covalently attached to the BV chromophore, is marked with asterisk. The chromophore surrounding residues within 4.5 Å, 4.5-5.5 Å and 5.5-6.5 Å are highlighted with gray, cyan, and green colors, respectively. The residues located in the dimer interface are highlighted with yellow. The introduced amino acids substitutions are highlighted in red. The residues located in the close proximity to the thioether linkage between BV and apoprotein are underlined. The α-helixes and β-sheets demonstrate the secondary structure of BphPs. The PAS, GAF and PHY domains are underlined with the blue, green, and red lines, respectively.

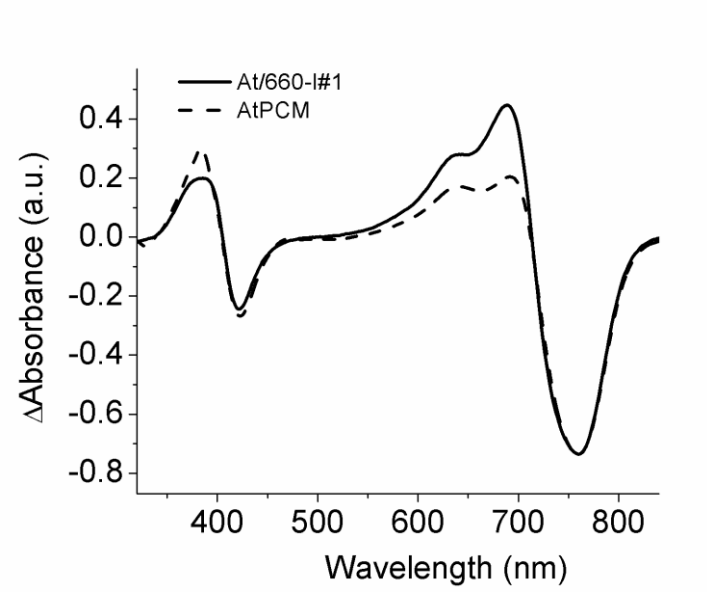

Supplementary Figure S13. Difference absorbance spectra of At/660-I#1 and AtPCD. Difference spectra "relaxed" minus "photoactivated" for At/660-I#1 (solid line) and AtPCD (dashed line). Photoactivation was performed by 60 mW/cm^2 of 750 nm LED light.

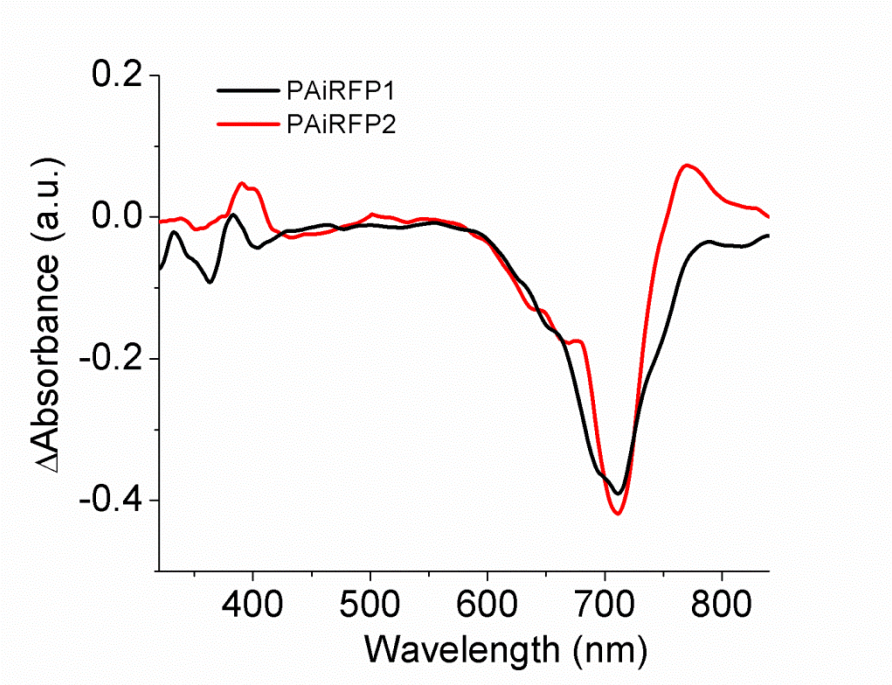

Supplementary Figure S14. Difference spectra for dark reversion of photoactivated PAiRFPs at low temperature.The "dark relaxation" minus "660 nm illumination" difference spectra for PAiRFP1 (black line) and PAiRFP2 (red line).

Supplementary Table S1. Spectral characteristics of AtPCD and its derivatives.

Protein	Mutations relative to AtPCD	$\lambda_{Pr/Pfr}$ (nm)	Em (nm)	$\tau_{1/2}$ (min)	PC[a] (fold)	ε_{Pr} ($M^{-1}cm^{-1}$)	QY (%)
AtPCD	none	699/758	713	0.18	1.8[b]	24,500	0.13[c]
At/660-I#1	R220P/V244F/A276V/ Y280C/E294V	693/758	717	4.1	3.1	70,000	3.7
At/660-II#9	R220P/V244F/A276V/ Y280C/E294V/A386V	693/758	717	4.6	4.0	79,000	3.5
At/660-III#8	R83K/R220P/V244F/A276V/ Y280C/E294V/A386V/ L419I/T469S	693/758	716	7.0	3.0	61,000	3.7
At/660-III#1	M163L/Q168L/R220P/ V244F/A276V/Y280C/ E294V/H303R/A386V	697/753	716	94	3.9	83,700	4.0
At/660-IV#2	G82S/R83K/M163L/Q168E/ R220P/V244F/A276V/Y280 C/E294V/A386V/L419I/T46 9S	693/753	720	82	9.0	62,800	4.3
At/660-IV2B	G127D/M163L/Q168L/ R220P/V244F/A276V/ Y280C/E294V/H303R/ A386V/A480V/H498Y	695/754	719	86	8.7	30,400	4.6
At/660-IV5D	K69R/R83K/G120D/A123T/ M163L/Q168E/R220P/V244 F/A276V/Y280C/E294V/A38 6V/G409D/L419I/T469S/A4 87T/E494G	696/754	717	354	3.6	36,300	4.7
PAiRFP1	G127D/S141R/M163L/Q168 L/A203V/G218S/R220P/V24 4F/A276V/Y280C/ E294V/H303R/A386V/ A480V/H498Y	693/751	717	58	9.0	67,100	4.8
PAiRFP2	K69R/R83K/G120D/A123T/ M163L/Q168E/R220P/S243 N/V244F/G269D/A276V/Y2 80C/V294A/H303F/H333R/I 336L/D349R/M351I/A386V/ G409D/L419I/T469S/A487T/ E494G	693/748	719	233	5.9	63,600	4.7

[a]PC, photoactivation contrast, was calculated as a ratio of fluorescence signals measured in same conditions before and after photoactivation of the protein; [b]Measured by absorbance changes at 758 nm; [c]Data from the ref[46]; $\lambda_{Pr/Pfr}$, maximum of absorbance of Pr (illuminated) and Pfr (relaxed) forms; Em, emission maximum of illuminated protein; $\tau_{1/2}$, half-time of dark reversion; ε_{Pr}, extinction coefficient of Pr (illuminated) form; QY, quantum yield of Pr (illuminated form).

Supplementary Table S2. Comparison of *in vitro* photoconversion properties of some GFP-like PAFPs with the similar characteristics of AtPCD and PAiRFPs.

Protein	Photoconversion light, nm	Photoconversion energy density, J/cm^2	Reference
PATagRFP	405/15	180±30	[45]
rsTagRFP	445/25	0.06±0.01	[39]
	570/30	6.0±0.1	
PSmOrange	489/30	168±9*	[38]
PAiRFP1	660/10	0.0350±0.0008	this paper
	760/10	0.0148±0.0004	
PAiRFP2	660/10	0.0340±0.0008	this paper
	760/10	0.0148±0.0004	

The photoconversion energy density was estimated as a product of time and light power intensity required for the protein photoconversion in a 50 μl cuvette at room temperature. *Measured in the presence of 5 mM of ferrocyanide as an oxidant.

Supplementary Note 1

Analysis of the PAiRFPs mutations.

The possible locations of the introduced mutations in the PAiRFPs tertiary structures were assumed as described in the main text, discussion section. The V244F and A276V mutations are common for both proteins and were introduced during the first round of mutagenesis (**Supplementary Table S1** and **Supplementary Fig. S4**). According to the amino acid sequence alignment (**Supplementary Fig. S12**) the F244 residue should locate in the close vicinity to 8-propionate side chain of the BV chromophore, while V276 resides near 12-propionate of BV. It was shown that interactions of the 12-propionate side chain with surrounding amino acids in *Dr*BphP from *Deinococcus radiodurans* was responsible for the ability to sense the ratio of "red" to "far-red" light.[49] The modification of the 8-propinate of BV generated multiple products in the Pfr state of *Dr*BphP[49]. However, neither 8- nor 12-propionate were essential for primary photoisomerization or dark reversion in *Dr*BphP.[49, 50] Indeed, the At/660-I#1 mutant retained the Pfr ground state and had an altered sensitivity of the "red" to "far-red" light ratio: it can be almost completely photoswitched into Pr under both 660 and 750 nm LED light (**Supplementary Fig. S3**). In addition, At/660-I#1 had slower rate of dark reversion as compared to AtPCD (**Supplementary Table S1**). Possibly, V244F and A276V mutations resulted in the ability to undergo Pfr→Pr photoconversion under both "red" and "far-red" light. The R220P, Y280C, and E294V substitutions, introduced during first round of random mutagenesis, may affect the rate of dark reversion. The combined effect of the R220P, V244F, A276V, Y280C, E294V mutations introduced during first round of random mutagenesis also appeared in dramatic increase of quantum yield of the Pr state from 0.13% to 3.7% (**Supplementary Table S1**).[46] In addition, the difference spectra for AtPCD and At/660-I#1 indicate the improvement in the Pfr→Pr photoconversion efficiency (**Supplementary Fig. S13**).

Another mutation in the chromophore binding pocket common for PAiRFP1 and PAiRFP2 is M163L. The M161 of *Pa*BphP that corresponds to L163 of PAiRFPs is located in the proximity to the conservative Y163 residue (**Supplementary Fig. S12**). In the *Pa*BphP Pfr structure, the hydroxyl group of Y163 forms a hydrogen bond with the propionate group of the BV ring C, an interaction that disappears upon photoconversion into Pr.[36] According to the *Pa*BphP structural and mutagenesis data Y163 is important for mediating the Pr→Pfr reaction.

The Y163H substitution disabled Pr→Pfr photoconversion under "red" light and significantly decreased the rate of dark reversion.[36] The substantially slower dark reversion was also observed after introduction of M163L mutation into At/660-II#9 and At/660-III#8 (**Table 1**). Therefore, possibly L163 in PAiRFPs can alter or hinder the interaction of Y163 with BV that causes increase in dark relaxation half-time and prevents the Pr→Pfr photoconversion.

Supplementary Note 2

Low temperature UV-visible spectroscopy.

To identify the intermediates involved into PAiRFPs photocycle we compared the calculated differences spectra for PAiRFPs photoconversion (**Fig. 2**) with the ones available for wild-type phytochromes.[14-17, 51] First, we analyzed the Pfr→Pr pathway for PAiRFPs. The difference spectra of "illuminated-relaxed" PAiRFPs in the "red" region could correspond to a mixture of the lumi-F and meta-Fa states with a different ratio, which is in agreement with previously reported data[47] (**Fig. 2b,d** and **Supplementary Fig. S1**). The most likely intermediates involved in the Pfr→Pr pathway for PAiRFPs under "red" and "far-red" light are identical. The difference spectra demonstrated peaks with the similar maxima supporting this hypothesis. However, at low temperature "far-red" 750 nm light caused more efficient Pfr photoconversion, which is also the case at room temperature (**Fig. 1k,l** and **Fig. 2b,d**).

Next, we checked if Pr can undergo phototransformation under red light. An appearance of the prominent band at ~746-749 nm after 660 nm illumination of the PAiRFPs Pr state at 77 K can indicate the formation of the lumi-R photoproduct (**Fig. 2f,h**). Subsequent decrease of the 702 nm absorbance band in darkness at 245 K correspond to the relaxation of the lumi-R state, the most likely, into the meta-Ra/Rc state (**Fig. 2e,g**). However, a slow thawing of meta-Ra/Rc led to the formation of the Pr state, without any noticeable admixture of Pfr. This indicates that the meta-Ra/Rc to Pfr transition is disabled. It should be noted that the difference spectra of "dark relaxed-660 nm" PAiRFPs had distinct profiles (**Fig. 2f,h**). The difference spectrum of PAiRFP2 had band with 770 nm maximum, which was absent in case of the PAiRFP1 difference spectrum. In addition the negative bands with maxima at 711 nm presented in both spectra had different shapes (**Supplementary Fig. S14**). We speculated that these differences in the spectra

profiles can be explained by formation of different intermediates. The peak at 770 nm of PAiRFP2 difference spectrum (**Fig. 2h**) possibly corresponds to meta-Rc, which typically has red shifted absorbance relatively to lumi-R[13]. In case of PAiRFP1 the "dark relaxed-660 nm" difference spectrum likely corresponds to meta-Ra. Therefore, we suggested that the Pr→Pfr phototransformation pathway is blocked at the meta-Ra→meta-Rc step in case of PAiRFP1, and meta-Rc→Pfr in case of PAiRFP2. It has been shown that formation and decay of meta-Rc are associated with chromophore deprotonation and protonation, respectively.[15, 48] Possibly, the introduced into PAiRFPs mutations disrupted the proton transfer pathway that disabled the meta-Ra→meta-Rc→Pfr transitions. It has been already shown that the Pr→Pfr photoconversion of BphPs can be arrested in the meta-Ra or meta-Rc states either by introduced mutations[35, 48, 52] or by chemical modification of BV.[53] Based on the obtained spectroscopic data we proposed possible photocycles for PAiRFP1 and PAiRFP2 (**Fig. 2i,j**).

Supplementary References

47. Spruit, C.J. & Kendrick, R.E. Phototransformations of phytochrome: the characterization of lumi-F and meta-Fa. *Photochem Photobiol* **26**, 133-138 (1977).
48. von Stetten, D. et al. Highly conserved residues Asp-197 and His-250 in Agp1 phytochrome control the proton affinity of the chromophore and Pfr formation. *J Biol Chem* **282**, 2116-2123 (2007).
49. Shang, L., Rockwell, N.C., Martin, S.S. & Lagarias, J.C. Biliverdin amides reveal roles for propionate side chains in bilin reductase recognition and in holophytochrome assembly and photoconversion. *Biochemistry* **49**, 6070-6082 (2010).
50. Rockwell, N.C., Shang, L., Martin, S.S. & Lagarias, J.C. Distinct classes of red/far-red photochemistry within the phytochrome superfamily. *Proc Natl Acad Sci U S A* **106**, 6123-6127 (2009).
51. Spruit, C.J.P. & Kendrick, R.E. Phototransormations of phytochrome: the characterization of Lumi-F and Meta-Fa. *Photochemistry and Photobiology* **26**, 133-138 (1977).
52. Yang, X., Stojkovic, E.A., Kuk, J. & Moffat, K. Crystal structure of the chromophore binding domain of an unusual bacteriophytochrome, RpBphP3, reveals residues that modulate photoconversion. *Proc Natl Acad Sci U S A* **104**, 12571-12576 (2007).
53. Seibeck, S. et al. Locked 5Zs-biliverdin blocks the Meta-RA to Meta-RC transition in the functional cycle of bacteriophytochrome Agp1. *FEBS letters* **581**, 5425-5429 (2007).